文章编号： 1008-9357(2025)03-0216-12 DOI： 10.14133/j.cnki.1008-9357.20250316001

# 主链-侧链协同工程增强聚合物光催化产氢

田昌昊[1]， 刘雪岩[1]， 虞苗杰[1]， 吴永真[1]， 车 瑜[2]， 张维伟[1]， 朱为宏[1]
（1. 华东理工大学化学与分子工程学院，上海 200237；2. 山西大学资源与环境工程研究所，太原 030006）

**摘 要：** 传统聚合物光催化剂通常采用芳香环构建基元以增强 π 共轭，然而其固有的疏水性和刚性结构导致其在水溶液中分散性较差，进而引发显著光学损失和激子复合。本研究创新性地将亲水性非共轭聚乙二醇（PEG）链段引入聚合物主链和侧链，设计并合成了 2 个系列共 6 种新型聚合物光催化剂（FLUSO, FLUSO-PEG10, FLUSO-PEG30；CPDTSO, CPDTSO-PEG10, CPDTSO-PEG30）。通过精确调控 PEG 链段的摩尔分数，在保持聚合物吸收能力的同时显著改善水分散性。实验结果显示优化后的 FLUSO-PEG10 表现出优异的光催化析氢速率，达到 33.9 mmol/(g·h)，较全共轭对应物提升近 3 倍。水接触角和粒径分析进一步证实，在主链中引入非共轭链段可增强聚合物/水界面相容性，抑制颗粒聚集，从而提升光催化剂的分散性，并促进电荷生成。

**关键词：** 有机半导体；聚合物光催化剂；主链工程；侧链工程；光催化析氢
**中图分类号：** O69 **文献标志码：** A

# Integrating Main-Chain and Side-Chain Engineering in Polymers for Enhanced Photocatalytic Hydrogen Production

TIAN Changhao[1], LIU Xueyan[1], YU Miaojie[1], WU Yongzhen[1], CHE Yu[2], ZHANG Weiwei[1], ZHU Weihong[1]
（1. School of Chemistry and Molecular Engineering, East China University of Science and Technology, Shanghai 200237, China; 2. Institute of Resources and Environmental Engineering, Shanxi University, Taiyuan 030006, China）

**Abstract:** Traditional polymeric photocatalysts are typically constructed using aromatic building blocks to enhance π-conjugation. However, their inherent hydrophobicity and rigid structure lead to poor dispersibility in aqueous solutions, resulting in significant optical losses and exciton recombination. In this study, two series of six novel polymer photocatalysts（FLUSO, FLUSO-PEG10, FLUSO-PEG30; CPDTSO, CPDTSO-PEG10, CPDTSO-PEG30）are designed and synthesized by incorporating the hydrophilic, non-conjugated polyethylene glycol (PEG) chain, into both the main and side chains of polymers. By precisely optimizing the ratio of hydrophilic PEG segments, the water dispersibility is significantly improved while the light absorption capability of the polymer photocatalysts is well maintained. The experimental results confirm that the optimized FLUSO-PEG10 exhibits excellent photocatalytic hydrogen evolution rate, reaching up to

**收稿日期：** 2025-03-16
**基金项目：** 国家自然科学基金 (T2488302, 22422805, 22338006, 92356301, 9235630033, 22375062)；上海市科学技术委员会 (24DX1400200, 24160711900)；上海市基础研究试点项目 (22TQ1400100-10)；中央高校基本科研业务费专项资金；上海市教育发展基金会、市教委“晨光计划”项目 (22CGA32)；CAST 青年精英科学家资助项目 (2023QNRC001)

**作者简介：** 田昌昊（2000—），男，安徽蚌埠人，硕士，主要研究方向为有机半导体光催化剂合成及其析氢性能研究。E-mail: 18855253574@163.com
**通信联系人：** 车 瑜，E-mail: yuche@sxu.edu.cn；张维伟，E-mail: zhangweiwei@ecust.edu.cn；朱为宏，E-mail: whzhu@ecust.edu.cn

**引用格式：** 田昌昊，刘雪岩，虞苗杰，吴永真，车 瑜，张维伟，朱为宏. 主链-侧链协同工程增强聚合物光催化产氢［J］. 功能高分子学报，2025，38(3)：216-227.
**Citation:** TIAN Changhao, LIU Xueyan, YU Miaojie, WU Yongzhen, CHE Yu, ZHANG Weiwei, ZHU Weihong. Integrating Main-Chain and Side-Chain Engineering in Polymers for Enhanced Photocatalytic Hydrogen Production［J］. Journal of Functional Polymers, 2025, 38(3): 216-227.

33.9 mmol/(g·h), which is nearly three times higher than that of fully π-conjugated counterparts. Water contact angles and particle size analyses reveal that incorporating non-conjugated segments into the main chains enhances the capacitance of the polymer/water interface and reduces particle aggregation, leading to improved photocatalyst dispersion and enhanced charge generation.

**Key words:** organic semiconductor; polymer photocatalyst; main-chain engineering; side-chain engineering; photocatalytic hydrogen evolution

Harnessing sunlight to generate hydrogen fuel through photocatalytic water splitting offers a promising pathway toward clean and sustainable energy[1, 2]. Organic semiconductors are particularly attractive for this process due to their strong absorption of visible light and highly tunable optoelectronic properties[3-6]. Among the extensively studied, organic photocatalysts are graphitic carbon nitrides (g-$C_3N_4$)[7-9], linear conjugated polymers (LCPs)[10-12], conjugated microporous polymers (CMPs)[13-15], and covalent organic frameworks (COFs)[16-19]. Typically, to enhance light absorption and charge transport, these photocatalysts are synthesized using rigid and aromatic building blocks, resulting in a planar, conjugated polymer network[20]. However, the inherent hydrophobicity of most aromatic building blocks, combined with difficulties in controlling the degree of polymerization, often leads to the formation of large polymer particles, ranging from microns to millimeters, in aqueous suspensions[4, 21, 22]. Since light can only penetrate organic semiconductors to a depth of a few hundred nanometers, such oversized particles are not fully activated by illumination[23, 24]. Moreover, as exciton diffusion lengths in organic semiconductors are usually limited to several tens of nanometers[25-27]. Thus, reducing the particle size and improving the water dispersion of organic photocatalysts are critical for enhancing their photocatalytic performance.

One effective strategy to enhance the water dispersibility of organic photocatalysts is by increasing their hydrophilicity, which improves wettability and minimizes agglomeration under ultrasonic dispersion process[28-30]. Common strategies in molecular engineering involve incorporating polar groups, such as sulfone moieties[31, 32], into the conjugated backbone or attaching hydrophilic side chains, including polyethylene glycol (PEG)[22, 33, 34], carboxylic acids[35], amino groups, or ionic electrolytes[36]. Nevertheless, despite these modifications, the polymer backbones typically remain hydrophobic. Recent study has demonstrated that introducing non-conjugated segments into the backbone can improve the water/polymer interface without significantly compromising light harvesting[37]. However, few reports have explored the simultaneous engineering of both the main chain and side chain in polymer photocatalysts, where achieving an optimal balance between non-conjugated and conjugated segments remains a critical challenge for enhancing hydrophilicity while maintaining efficient charge transport.

Here, we developed two series of hydrophilic polymer photocatalysts (FLUSO and CPDTSO) by integrating both main-chain and side-chain engineering. Hydrophilic PEG groups were simultaneously grafted onto π-conjugated fluorene (FLU) or cyclopentadithiophene (CPDT) building blocks, and incorporated into the polymer main chain as non-conjugated segments. By carefully optimizing the ratio of non-conjugated segments, their photophysical properties were well maintained as compared to those of the fully π-conjugated polymer. Remarkably, FLUSO-PEG10 achieved an enhanced photocatalytic hydrogen evolution rate of 33.9 mmol/(g·h) under visible light irradiation, approximately three times higher than that of the fully π-conjugated one with only hydrophilic side chains. Water contact angle test and scanning electron microscopy (SEM) image indicated that introducing PEG into the polymer main chain reduced the contact angle, resulting in significantly less particle aggregation in the photocatalytic solution. This reduction in particle size enhanced catalytic sites and improved charge generation which was confirmed by transient photocurrent tests.

# 1 Experiment

## 1.1 Chemicals

All reagents were obtained from Macklin, Meryer, Boer and used as received. Solvents were obtained from

commercial sources and used without further purification.

### 1.2 Synthesis of Polymer Photocatalysts

All polymers were synthesized by Pd-catalyzed Suzuki-Miyaura coupling reaction. 3,7-Dibenzo[b,d]thiophene sulfone diboronic acid bis(pinacol) ester (mole fraction 100%), PEG substituted 2,7-dibromo-9 H-fluorene or 2,6-dibromo-4H-cyclopenta-[2,1-b:3,4-b']dithiophene (mole fraction 100%, 90% and 70%), 1,11-di(4-bromophenoxy)-3,6,9-trioxaundecane (mole fraction 0, 10% and 30%), $Pd(PPh_3)_4$ (mole fraction 3.6%), and $K_2CO_3$ (2 mol/L, 5.6 mL) were added to a dried Schlenk tube. THF was added via syringe and the solution was dried under vacuum for 5 min and then purged with $N_2$. The mixture was stirred under nitrogen at 85 ℃ overnight. After cooling to room temperature, the mixture was poured into methanol and washed with methanol, *n*-hexane and water after filtration to afford the target polymer FLUSO, FLUSO-PEG10, FLUSO-PEG30, CPDTSO, CPDTSO-PEG10 and CPDTSO-PEG30 (Yield: 59.2%, 51.1%, 64.3%, 66.3%, 61.6% and 56.0%), respectively.

### 1.3 Characterization

$^1$H-nuclear magnetic resonance (NMR) spectra were recorded in solution at 400 MHz, using a Bruker Avance 400 NMR spectrometer. UV-Visible (UV-Vis) absorption spectra were collected on a Varian Cary 500 spectrophotometer. The optical bandgap ($E_g$) was obtained from Tauc plots of the UV-Vis spectra and by extrapolation of the linear part of the curve to the energy axis based on the relationship $\alpha h\nu = A(h\nu - E_g)^{\gamma}$, where $\alpha$ is the absorption coefficient, $A$ is an energy-independent constant, $E_g$ is the optical bandgap, $h$ is Planck's constant, $\nu$ is the velocity, and $\gamma$ is a constant representing the type of electronic transition. Fluorescence spectra were recorded on Edinburgh Instrument (2 Bain Square, Kirkton Campus, Lovingston, UK). Fourier transform infrared spectrometer (FT-IR) was acquired on Thermo Nicolet Corporation (7 800-350/cm 0.01/cm/6 700). X-ray photoelectron spectroscopy (XPS) data were measured in powder form using an ESCALAB 250 Xi instrument (Thermo Fisher Scientific) with a monochromatized Al K$\alpha$ line source. The photoelectric data of samples were recorded by the CHI660 B electrochemical workstation of (Shanghai Chenhua, China). A standard three-electrode system was employed with a platinum foil and Ag/AgCl as the counter electrode and the reference electrode, respectively. The working electrodes were prepared as follows: Typically, polymer dispersion was mixed with Nafion (1 mL, volume fraction 4%) under the ultrasonication for 30 min. Then, 0.1 mL of the suspension was dropwise coated on the indium tin oxide (ITO) glass substrate for three times. 0.2 mol/L $Na_2SO_4$ aqueous solution was employed as the electrolyte. The polymer dispersions were drop-coated onto ITO glass for three times to make films, and the water contact angle measurements were performed by JC2000 C (Power Each). The morphologies of polymers were imaged using a field-emission scanning electron microscope (Helios G4 UC, Thermo Fisher Scientific). Transmission electron microscopy characterizations were performed on a Themis *Z* microscope (Thermo Fisher Scientific) equipped with two aberration correctors under 200 kV. Samples were cast on a copper grid with holey carbon supporting films. Scanning transmission electron microscopy and element mapping were collected on a Talos F200 X transmission electron microscope.

### 1.4 Photocatalytic Hydrogen Evolution Measurement

Photocatalytic hydrogen evolution experiments were conducted in a glass system (250 mL). Typically, a quartz reactor was charged with polymer dispersion (25 mL) containing 2.5 mg catalysts, ascorbic acid (0.2 mol/L), and a certain amount of Pt as a cocatalyst using hexachloroplatinic acid as a Pt precursor. Before light irradiation, the dissolved air was thoroughly removed by bubbling with $N_2$ for 30 min. Then the system was irradiated from the top using a 300 W xenon lamp (Perfectlight PLS-SXE300 D). The temperature of the reaction solution was maintained at 20 ℃ by circulation of cool water. The evolved gases were detected on a gas chromatograph (Shimadzu GC 2014 C) with a thermal conductive detector.

## 2 Results and Discussion

Two series of polymer photocatalysts (FLUSO and CPDTSO) were constructed using fluorene (FLU) or

cyclopentadithiophene (CPDT) as electron donors and dibenzothiophene sulfone (DTSO) as electron acceptors. Polymers based on fluorene and cyclopentadithiophene have been reported to exhibit excellent properties such as high coplanarity and electrical conductivity, attributed to their rigid and planar molecular structures[38]. These structural characteristics contribute to a narrower bandgap and superior light-harvesting capabilities, both of which are highly desirable for photocatalytic applications. The dibenzothiophene sulfone (DTSO) unit was selected due to its strong electron-withdrawing nature, planar geometry, and the high hydrophilicity conferred by the sulfone group. These features make DTSO a widely used building block in the design of efficient organic photocatalysts[39]. We employed both main-chain and side-chain engineering by incorporating penta(ethylene glycol) (PEG) into the backbone as well as the side chains of FLUSO and CPDTSO (Fig. 1). The PEG-based hydrophilic non-conjugated segments were integrated into the main chain via a one-pot Pd-catalyzed Suzuki-Miyaura coupling polymerization, simply by replacing the dibromo-monomers with PEG-functionalized (PEG-Br) segments. By varying the mole fractions (0, 10% and 30%) of these hydrophilic non-conjugated segments, six polymer photocatalysts, FLUSO, FLUSO-PEG10, FLUSO-PEG30, CPDTSO, CPDTSO-PEG10 and CPDTSO-PEG30 were synthesized (Fig. 1).

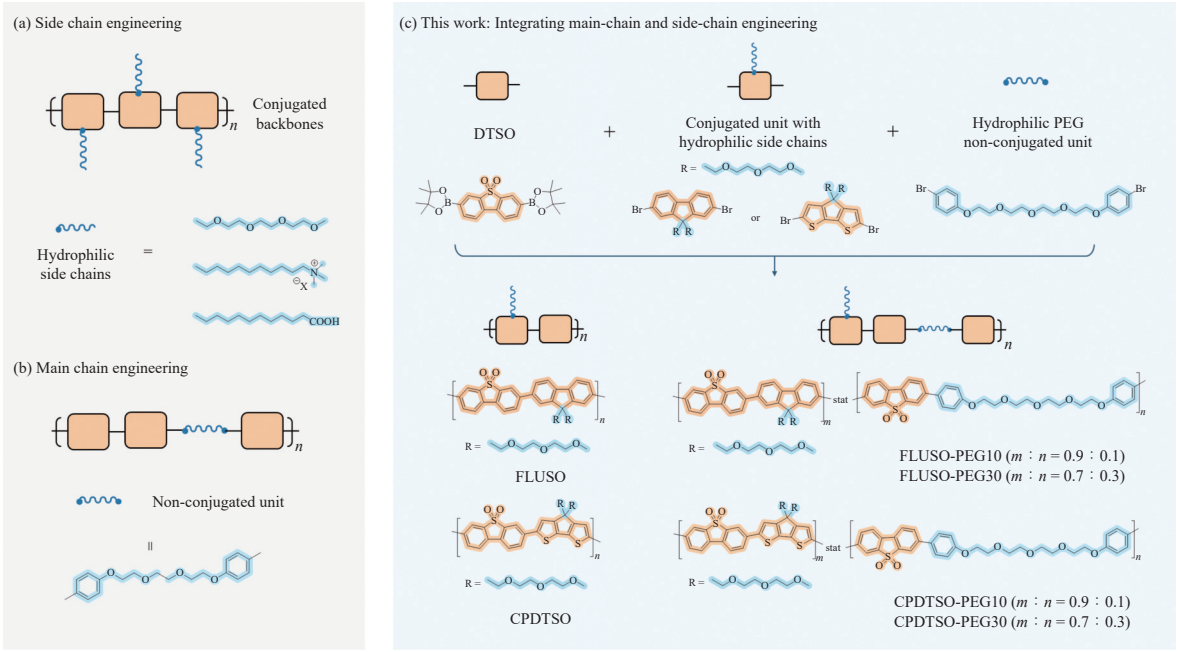


Fig. 1　Schematic illustration of hydrophilicity design strategy and the chemical structures of polymer photocatalysts

The chemical structures of the synthesized polymers were confirmed using Fourier-transform infrared (FT-IR) spectroscopy and X-ray photoelectron spectroscopy (XPS). In the FT-IR spectra, FLUSO showed peaks at 1 602 $cm^{-1}$ and 1 456 $cm^{-1}$ (Fig. 2(a)), which are attributed to the C=C stretching vibrations of the phenyl group in the polymer backbone. Additional peaks at 1 304 $cm^{-1}$ and 1 157 $cm^{-1}$ correspond to the characteristic stretching vibrations of the O=S=O group, which confirms the presence of the sulfone moiety. The spectra also revealed two distinct C－H stretching vibration peaks in the range of 2 800～3 000 $cm^{-1}$, along with asymmetric C－O－C stretching peaks between 1 000 $cm^{-1}$ and1 170 $cm^{-1}$, which verify the incorporation of PEG side chains (Fig. 2(a)). When PEG-based hydrophilic non-conjugated segments were incorporated into the polymer main chain, as in FLUSO-PEG10 and FLUSO-PEG30, the FT-IR spectra remained similar to that of FLUSO. For the CPDTSO polymers, aside from the similar sulfone group signals (1 304 $cm^{-1}$ and 1 153 $cm^{-1}$)[40], a distinctive C－S stretching band emerged at 706 $cm^{-1}$, which is attributed to the CPDT unit[37] (Fig. 2(b)). The XPS survey spectra indicated that these polymers contain carbon, oxygen, and sulfur elements. The high-resolution C 1s spectra (Fig. 2(c)) can be deconvoluted into three peaks at 284.8, 285.3 eV and 286.4 eV, which correspond to C=C, C－S, and C－O－C bonds, respectively. While the C 1s spectra of FLUSO and CPDTSO are similar, their S 2p signals differ significantly (Fig. 2(d)). FLUSO polymers showed

a single set of S 2p peaks at 169.4 eV and 168.2 eV, corresponding to the 2 $p_{1/2}$ and 2 $p_{3/2}$ states of R—$SO_2$—R[41]. In contrast, CPDTSO polymers exhibited an additional set of S 2p signals at 165.2 eV and 164.0 eV, corresponding to the 2 $p_{1/2}$ and 2 $p_{3/2}$ states of R—S—R from the CPDT unit[42].

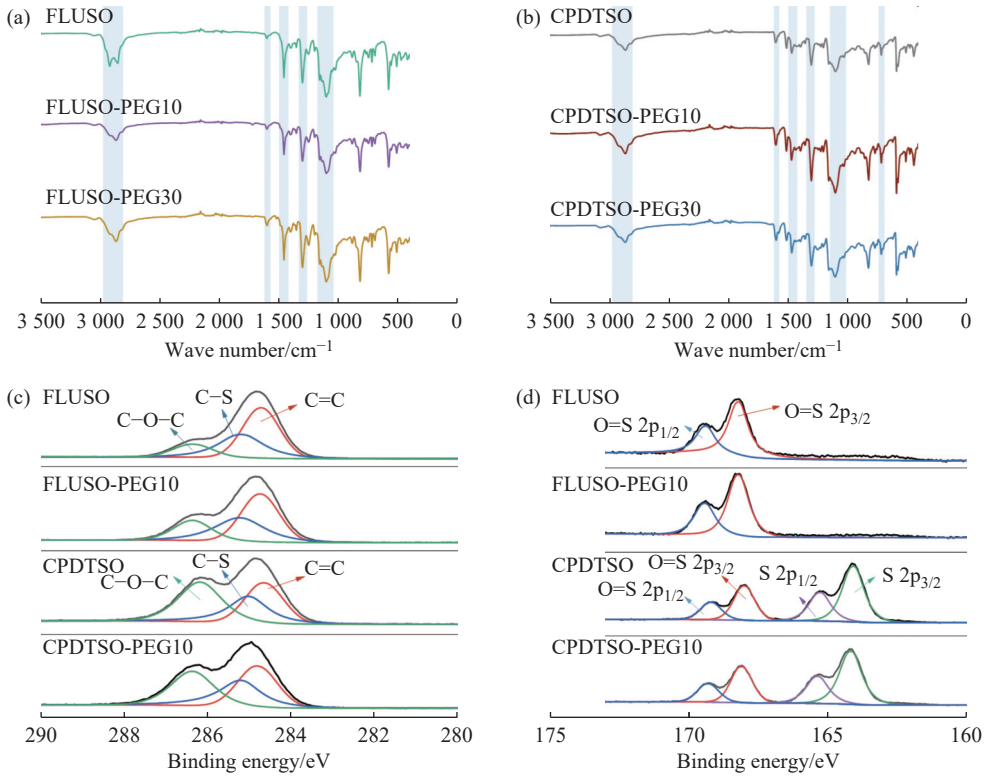


Fig. 2 FT-IR spectra of (a) FLUSO based polymers and (b) CPDTSO based polymers; (c) C 1s and (d) S 2p XPS spectra of FLUSO based polymers and CPDTSO based polymers

The photophysical properties of these polymers photocatalysts were investigated using UV-Vis diffuse reflectance spectroscopy and photoluminescence (PL) spectroscopy. As shown in Fig. 3(a), FLUSO exhibited a broad absorption band from 300 nm to 500 nm with an absorption edge around 600 nm. In contrast, CPDTSO, owing to the stronger electron-donating ability of the cyclopentadithiophene unit compared to fluorene, exhibits a significantly red-shifted absorption band extending from 300 nm to 650 nm, with the absorption edge shifting to approximately 700 nm. FLUSO-PEG and CPDTSO-PEG polymers displayed absorption bands similar to their fully π-conjugated analogues, albeit with a slight blue shift in the absorption edge, likely due to reduced aggregation of the polymer backbones. Furthermore, solid-state PL measurements suggested a red-shifted emission peak of CPDTSO compared with FLUSO (680 nm vs 550 nm, Fig. 3(c)). After incorporating the non-conjugated segments, FLUSO-PEG showed a slight blue shift in their emission peaks relative to FLUSO, while the emission peak of CPDTSO-PEG was similar to CPDTSO.

The energy levels of the polymer photocatalysts were estimated using a combination of Mott-Schottky analysis and Tauc plots. The maximum absorption wavelength ($\lambda_{max,\ abs}$) was determined by Tauc plots derived from the absorption spectra (Fig. 3(b)), with $E_g$ values of 2.56, 2.58, 2.63, 1.92, 1.94 eV, and 1.95 eV for FLUSO, FLUSO-PEG10, FLUSO-PEG30, CPDTSO, CPDTSO-PEG10, and CPDTSO-PEG30, respectively. The flat band potentials ($E_{fb}$) were determined versus Ag/AgCl based on the Mott-Schottky formula and the conduction band ($E_{CB}$) potentials were −0.77, −0.74, −0.71, −1.01, −0.85 V and −0.99 V versus the normal hydrogen electrode ($E_{NHE}$) for FLUSO, FLUSO-PEG10, FLUSO-PEG30, CPDTSO, CPDTSO-PEG10 and CPDTSO-PEG30, respectively, calculated using the equations $E_{CB} = E_{fb}$+0.1 V and $E_{NHE}=E_{Ag/AgCl}$+0.2 V. The valence band ($E_{VB}$) levels were then calculated using the equation $E_{VB} = E_g+E_{CB}$[43], resulting in $E_{VB}$ values ranging from 1.79 V to 1.92 V for FLUSO polymers and from 0.91 V to 1.09 V for the CPDTSO polymers (Fig. 3(d)). The photophysical properties for FLUSO and CPDTSO polymers were shown in Table 1.

The molecular electrostatic potential (ESP) of the repeat units of FLUSO and CPDTSO polymers was investigated to visualize the spatial distribution of positive and negative charges, which is critical for understanding and predicting intermolecular interactions[44, 45]. As shown in Fig. 3(e), the negative charges in FLUSO are distributed on both the electron-withdrawing sulfone group and the benzene ring of the FLU unit, while the negative charges in CPDTSO are primarily localized on the sulfone group due to the stronger electron-donating properties of the incorporated CPDT group. Additionally, the spatial distributions of the lowest unoccupied molecular orbital (LUMO) and the highest occupied molecular orbital (HOMO) in these polymers were studied using density functional theory (DFT) calculations (Fig. 3(f, g)). All DFT calculations and ESP analyses were performed with the CAM-B3 LYP density functional, with def2 SVP basis set using the Gaussian 16 and Multiwfn software[46, 47]. FLUSO and CPDTSO polymers exhibit similar LUMO distributions, with electron density predominantly populates on the sulfone unit. In the HOMO state, the electron density is largely concentrated on their donor moiety and the conjugated aromatic nucleus. This behavior is characteristic of donor-acceptor (D-A) polymers, theoretically promoting the migration of photogenerated charge. These provide a strong foundation for further main-chain and side-chain engineering on polymer backbones.

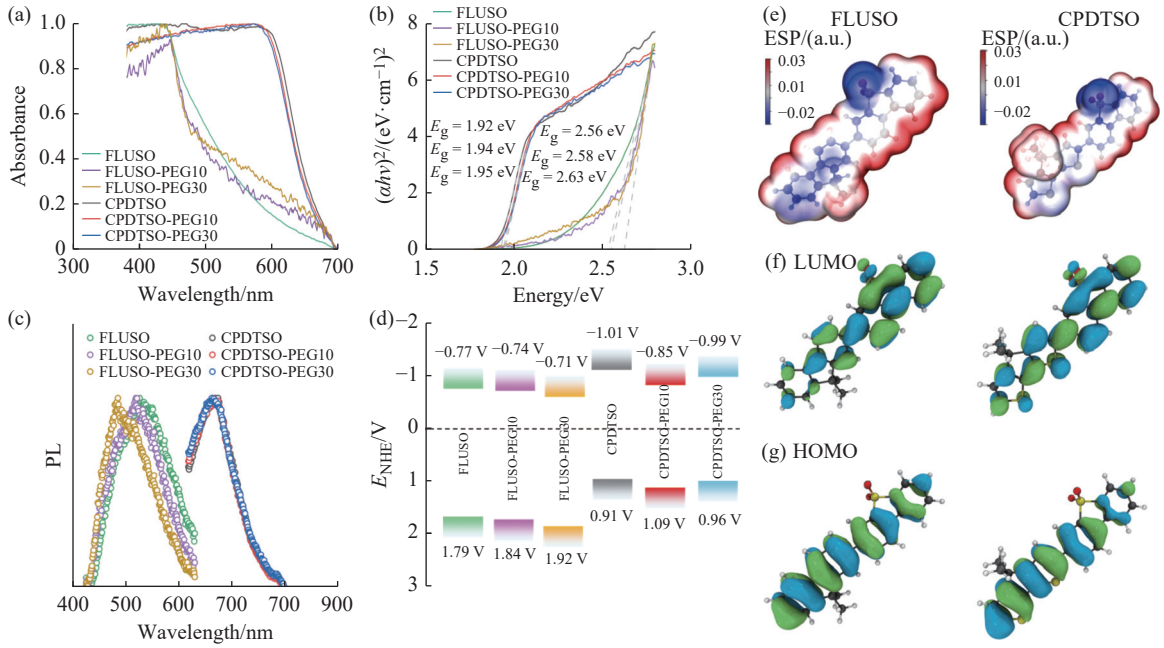


Fig. 3　(a) Solid-state UV-Vis diffuse reflectance spectra; (b) Tauc plots; (c) Solid-state photoluminescence spectra ($\lambda_{ex}$ = 350 nm for FLUSO based polymers and $\lambda_{ex}$ = 500 nm for CPDTSO based polymers); (d) Energy level diagram of all prepared polymers; (e) Electrostatic potential; (f) LUMO and (g) HOMO distribution of the molecular fragments in FLUSO and CPDTSO polymer as models (Gray, light gray, yellow and red balls refer to C, H, S and O atoms, respectively)

Table 1　The photophysical properties for FLUSO and CPDTSO polymers

| Polymer | $\lambda^{1)}_{max,abs}$/nm | $E^{2)}_{fb}$/V | $E^{3)}_{NHE}$/V | $E^{4)}_{VB}$/V | $E^{5)}_{CB}$/V | $E^{6)}_{g}$/eV |
|---|---|---|---|---|---|---|
| CPDTSO | 646 | −1.11 | −0.91 | 0.91 | −1.01 | 1.92 |
| CPDTSO-PEG10 | 639 | −0.95 | −0.75 | 1.09 | −0.85 | 1.94 |
| CPDTSO-PEG30 | 636 | −1.09 | −0.89 | 0.96 | −0.99 | 1.95 |
| FLUSO | 484 | −0.87 | −0.67 | 1.79 | −0.77 | 2.56 |
| FLUSO-PEG10 | 481 | −0.84 | −0.64 | 1.84 | −0.74 | 2.58 |
| FLUSO-PEG30 | 471 | −0.81 | −0.61 | 1.92 | −0.71 | 2.63 |

1) Determined by solid-state UV-Vis diffuse reflectance spectroscopy; 2) Determined versus Ag/AgCl based on the Mott-Schottky formula; 3) Determined by the equation $E_{NHE}$= $E_{Ag/AgCl}$+0.197 V; 4) Determined by the equation $E_{VB} = E_{CB}+E_g$; 5) For many *n*-type semiconductors, $E_{fb}$ is considered to be about 0.1 V more positive than its conduction band potentials; 6) Determined from Tauc plots

We next evaluated the photocatalytic hydrogen evolution performance of these polymers using platinum (Pt) as a co-catalyst in a $H_2O$/MeOH/TEA (volume ratio 1:1:1) mixture, where TEA (triethylamine) serves as the sacrificial electron donor and MeOH helps mix TEA with water. As shown in Fig. 4(a), 2.5 mg of FLUSO polymer generated 163.7 μmol of $H_2$ over 5 h of photolysis under visible light irradiation, corresponding to a hydrogen evolution rate (HER) of 32.7 μmol/h (13.1 mmol/(g·h) when normalized to gram-scale). In contrast, CPDTSO exhibited a much lower HER of 3.4 μmol/h (1.3 mmol/(g·h)), approximately one-tenth of FLUSO, despite its broader absorption spectrum. This discrepancy may arise from the insufficient driving force for TEA oxidation due to the upward-shifted $E_{VB}$ of CPDTSO. Since holes transfer from the photoexcited polymer to TEA constitutes the initial step in the photocatalytic process[48], the reduced thermodynamic driving force limits the ability of TEA to effectively scavenge photogenerated holes, thereby diminishing overall photocatalytic performance[49]. Remarkably, when 10% (mole fraction) hydrophilic non-conjugated segments were incorporated, FLUSO-PEG10 and CPDTSO-PEG10 produced 424.1 μmol and 24.9 μmol of $H_2$, respectively, under the identical catalytic conditions, with average HER of 33.9 mmol/(g·h) and 2.0 mmol/(g·h). These values are nearly 3 and 2 times higher than those of their fully conjugated counterparts, FLUSO and CPDTSO. Further increasing the proportion of non-conjugated segments to 30% (mole fraction) led to an increased HER for CPDTSO-PEG30 (25.1 μmol/h, 6.1 mmol/(g·h)), while there was only minor improvement for FLUSO-PEG30 (61.6 μmol/h, 24.6 mmol/(g·h)). These results emphasize the advantage of hydrophilic non-conjugated main-chain engineering in enhancing photocatalytic performance.

The photocatalytic activity of the best-performing polymer, FLUSO-PEG10, was also tested under AM 1.5 G filter irradiation, which achieved a HER of 22.3 mmol/(h·g) (Fig. 4(b)). A control experiment was performed by removing light irradiation, where no hydrogen evolution was detected, supporting that it is a photocatalytic process mediated by the polymers. Further testing of FLUSO-PEG10 with various sacrificial agents revealed that TEA provided the highest performance, while only minimal hydrogen was produced with ascorbic acid (AA) and triethanolamine (TEOA), probably due to the slower oxidation kinetics for these sacrificial agents (Fig. 4(c)). Additionally, two repeated batches of FLUSO-PEG10 were tested, which showed negligible differences in photocatalytic activities (Fig.4(d)), demonstrating high reproducibility for the photocatalysis test.

Apparent quantum yield (AQY), which indicates the conversion efficiency of incident photons to hydrogen, was measured for FLUSO-PEG10. The parameters required for AQY calculation were shown in Table 2. As displayed in Fig. 4(e), FLUSO-PEG10 exhibited AQY of 23.2%, 17.3%, and 2.8% at 400, 420 nm and 475 nm, respectively, which aligns well with its absorption spectrum and supports its high hydrogen evolution rate. The long-term stability of FLUSO-PEG10 was assessed through five consecutive photocatalytic cycles under visible light irradiation (Fig. 4(f)). The HER remained stable throughout all cycles with 95% of the initial rate retained in the final cycle, demonstrating good photocatalytic stability were measured for FLUSO-PEG10.

Since FLUSO-PEG10 possessed similar photophysical properties to fully π-conjugated counterparts, we hypothesize that the enhanced photocatalytic activity may stem from differences in their water/polymer interface. The hydrophilicities of these polymers were assessed by measuring the water contact angles of their polymer films. The polymer dispersions were drop-coated onto ITO glass for three times to make films and the water contact angle measurements were performed by JC2000C (Power Each). As shown in Fig. 5(a～c), FLUSO displayed water contact angles of 94°. When a small mole fraction (10%) of hydrophilic, non-conjugated segments was introduced into FLUSO, FLUSO-PEG10 showed a significant decrease in the water contact angle to 65°. Further increasing the proportion of PEG non-conjugated segments in the main chain led to minimal change in the water contact angles. The observed variation in water contact angles correlates well with the photocatalytic hydrogen evolution rate, suggesting that the improved water/polymer interface is beneficial for photocatalytic hydrogen production.

The nano-morphologies of FLUSO polymers dispersed in photocatalysis solution were analyzed using SEM. As shown in Fig. 5(d～f), FLUSO exhibited a bulk morphology with significant particle aggregation, with dimensions reaching hundreds of micrometers. In contrast, FLUSO-PEG10 and FLUSO-PEG30 exhibited loosely aggregated

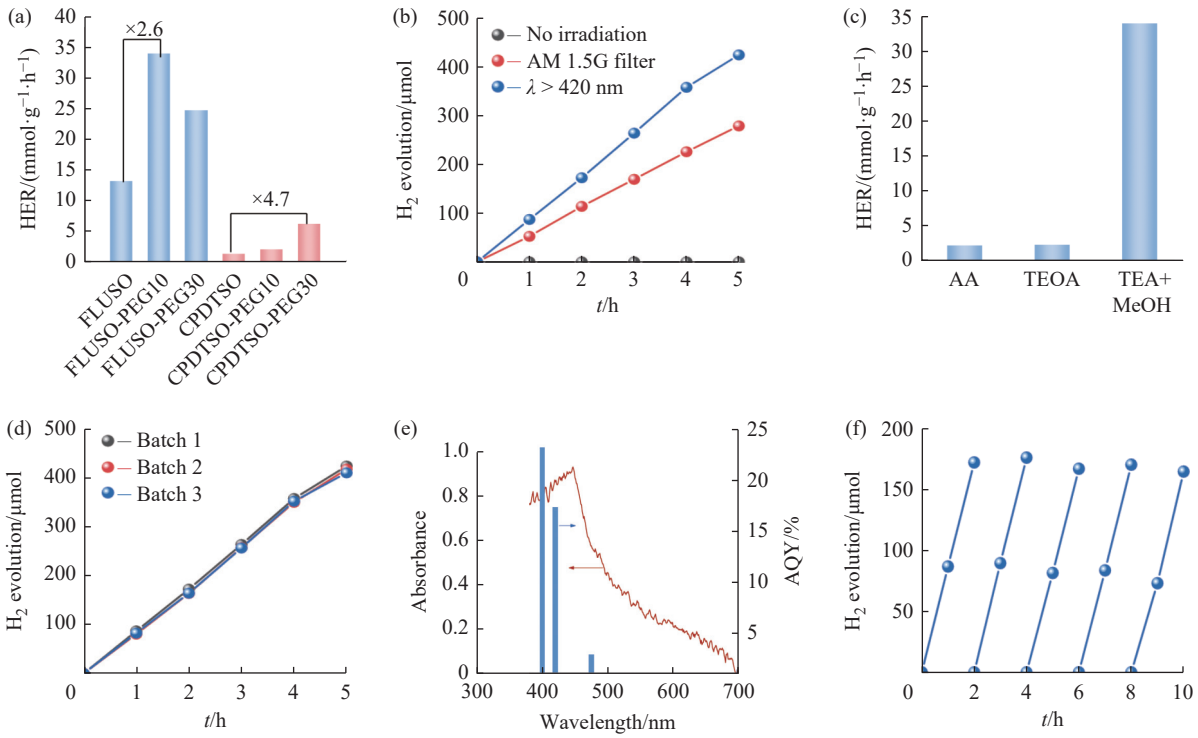


Fig. 4　(a) Photocatalytic hydrogen evolution rates for FLUSO based polymers and CPDTSO based polymers under visible light irradiation ($\lambda$ > 420 nm); (b) Time-dependent photocatalytic hydrogen evolution for FLUSO-PEG10 under visible light ($\lambda$ > 420 nm), AM 1.5 G filter irradiation and without irradiation; (c) Photocatalytic hydrogen evolution rates for FLUSO-PEG10 using different sacrificial agents under visible light irradiation ($\lambda$ > 420 nm); (d) Photocatalytic hydrogen evolution rates for FLUSO-PEG10 tested for different batches under visible light irradiation ($\lambda$ > 420 nm); (e) The absorption spectra and apparent quantum yields (AQY) for FLUSO-PEG10 at 400, 420 nm, and 475 nm, respectively; (f) Long-term photocatalytic hydrogen evolution for FLUSO-PEG10 under visible light irradiation ($\lambda$ > 420 nm) (the system was degassed again between each cycle) (Photocatalysis conditions: 2.5 mg photocatalyst, 25 mL MeOH/TEA/$H_2O$ (volume ratio 1∶1∶1), Pt based on polymer nanoparticles mass as co-catalyst)

Table 2　Parameters required for apparent quantum yield (AQY) calculation

| $H_2$ evolution/μmol | Irradiated area/cm$^2$ | $t$/s | Average light intensity/(mW·cm$^{-2}$) | Wavelength/nm | AQY/% |
|---|---|---|---|---|---|
| 46.3 | 18.1 | 3 600 | 1.83 | 400 | 23.2 |
| 45.3 | 18.1 | 3 600 | 2.28 | 420 | 17.3 |
| 11.5 | 18.1 | 3 600 | 3.18 | 475 | 2.8 |

nanostructures composed of smaller particles. This behavior can be attributed to the replacement of π-conjugated aromatic units with non-conjugated PEG segments, which helps reduce the strong aggregation and packing of aromatic backbones. The modified nano-morphology of FLUSO-PEG10 remained stable during photocatalysis reaction. Post-photocatalysis characterization using scanning transmission electron microscopy (STEM) revealed that the morphology of FLUSO-PEG10 remained unchanged, maintaining its loosely packed, small, and dispersed particle structures (Fig. 5(g, h)). The Pt co-catalyst, deposited via photoreduction, was uniformly distributed throughout the polymer, exhibiting a consistent particle size of less than 5 nm. Elemental mapping (Fig. 5(i)) confirmed the presence of Pt signals from the photo-deposition of co-catalyst, which further supported the chemical stability of FLUSO-PEG10 following photocatalysis.

To examine the effect of main-chain and side-chain engineering on the dispersibility of polymer photocatalysts, the particle size distributions were further analyzed by measuring UV-vis absorption spectra after sonication dispersion in a photocatalytic solution and filtration through filters with varying pore sizes. This method was chosen due to the polydispersity of the insoluble polymers, which makes measurement via dynamic light scattering (DLS) or static light scattering (SLS) challenging. As seen in Fig. 5(j, k), the FLUSO dispersion displayed an absorption band in the

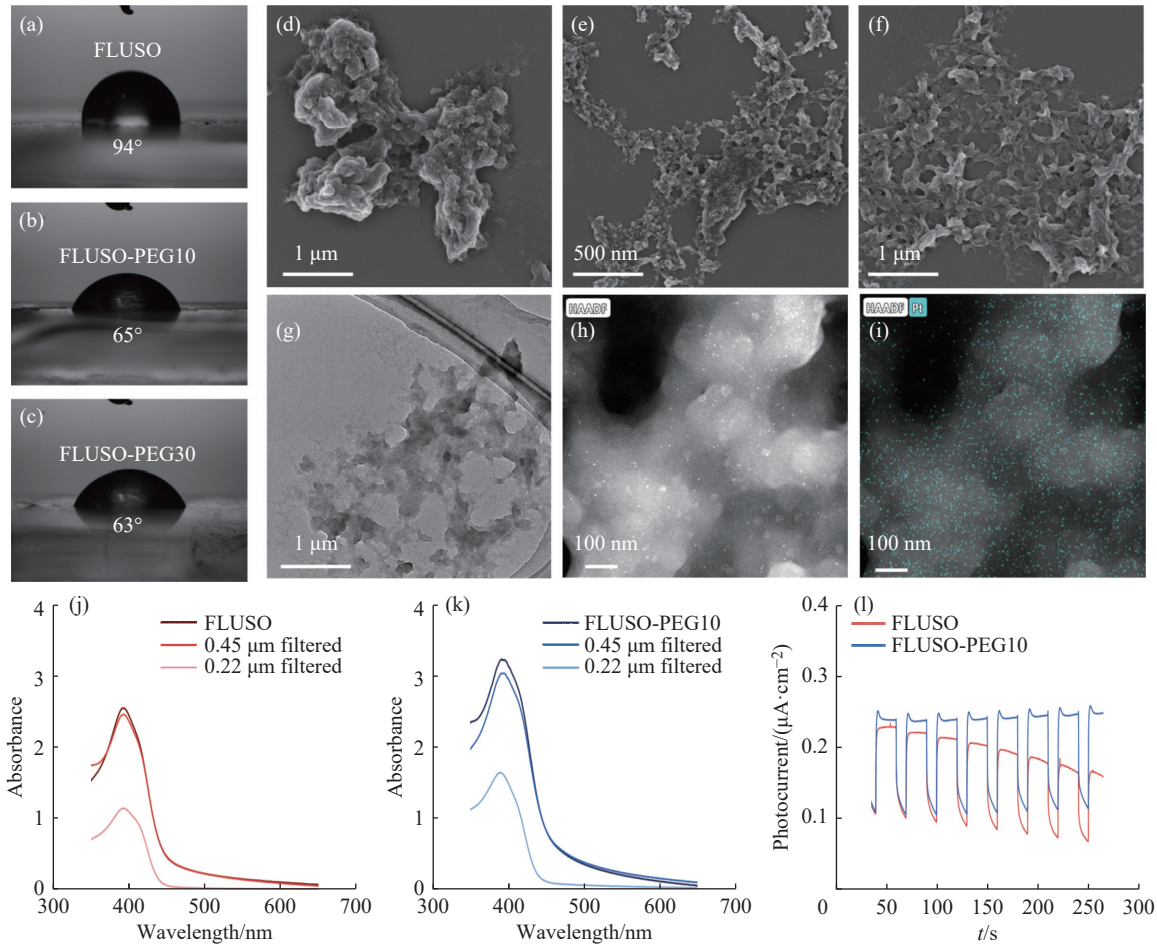


Fig. 5 Water contact angles of (a) FLUSO, (b) FLUSO-PEG10 and (c) FLUSO-PEG30 as thin films; SEM images of (d) FLUSO, (e) FLUSO-PEG10 and (f) FLUSO-PEG30 dispersion in $H_2O$/MeOH/TEA (volume ratio 1∶1∶1); (g) TEM image; (h) HAADF-STEM image and (i) EDX mapping analysis of platinum for FLUSO-PEG10 after photocatalytic reaction; Absorption spectra of (j) FLUSO, (k) FLUSO-PEG10 polymers dispersed in $H_2O$/MeOH/TEA (volume ratio 1∶1∶1) and filtered using Nylon filters with pore sizes of 0.45 μm and 0.22 μm; (l) Transient photocurrents of FLUSO and FLUSO-PEG10

300～450 nm, with tails extending to 600 nm, consistent with their solid-state absorption spectra. Notably, FLUSO-PEG10 exhibited a significantly higher absorption intensity compared to FLUSO, despite both being dispersed at the same concentration. The increased absorption intensity can be attributed to the reduced particle size and enhanced dispersion of FLUSO-PEG10 in photocatalytic solutions. After filtration through a 0.45 μm filter, the absorbance of all polymer dispersions remained largely unchanged, indicating that most particles are smaller than 0.45 μm, highlighting the effectiveness of hydrophilic side-chain engineering. When filtered through a 0.22 μm filter, the FLUSO dispersion retained less than 40% of its original absorbance, whereas the FLUSO-PEG10 dispersions retained more than 50%, suggesting a greater proportion of particles smaller than 0.22 μm. Therefore, the introduction of non-conjugated PEG in the main polymer chains facilitates the formation of smaller particles, resulting in better dispersion in the photocatalytic solution and enhanced light absorption. It is important to note that the particle size estimates from the UV-Vis absorption measurements may not fully correlate with photocatalytic activity, as the nano-morphologies and reaction kinetics also play crucial roles in the surface-dominated photocatalytic reaction.

The charge generation of polymers with main-chain and side-chain engineering was studied by transient photocurrent. As displayed in Fig. 5(l), by incorporating non-conjugated PEG in the polymer main chains, FLUSO-PEG10 showed a higher and more stable photocurrent response than FLUSO under light illumination, suggesting the more efficient charge generation. Overall, the enhanced photocatalytic hydrogen production for FLUSO-PEG10 can be attributed to the optimized hydrophilicity and dispersion in photocatalysis solutions, which reduces the distance that

excitons need to travel.

## 3 Conclusion

In summary, we have successfully developed two series of hydrophilic polymer photocatalysts by integrating main-chain and side-chain engineering for enhanced photocatalytic hydrogen production. By progressively integrating hydrophilic PEG chains into the FLU and CPDT building blocks, as well as the conjugated backbone, the resulting photocatalysts retained photophysical properties similar to their fully conjugated counterparts, with no significant loss in light absorption. Notably, the inclusion of the hydrophilic, non-conjugated segments in the polymer main chain greatly enhanced photocatalytic hydrogen evolution activity, with FLUSO-PEG10 achieving an average hydrogen evolution rate of 33.9 mmol/(g·h), nearly three times higher than those of fully conjugated FLUSO. Water contact angle measurements confirmed an improved water/polymer interface upon the introduction of non-conjugated PEG segments. Particle size distribution analysis indicated decreased particle size and aggregation of FLUSO-PEG10 in the photocatalytic solution, accompanied by enhanced dispersion and light absorption. This reduction in particle size promoted charge generation, thereby improving the photocatalytic performance.

## Acknowledgements

We acknowledge the Research Center of Analysis and Test of East China University of Science and Technology (ECUST) for assistance with various characterizations.

**参考文献:**

[1] ZHOU P, NAVID I A, MA Y, XIAO Y, WANG P, YE Z, ZHOU B, SUN K, MI Z. Solar-to-hydrogen efficiency of more than 9% in photocatalytic water splitting[J]. Nature, 2023, 613: 66-70.

[2] ZHOU Q X, GUO Y, ZHU Y F. Photocatalytic sacrificial $H_2$ evolution dominated by micropore-confined exciton transfer in hydrogen-bonded organic frameworks[J]. Nat Catal, 2023, 6: 574-584.

[3] ZHANG W W, JIANG H Y, YU M J, WANG J, SHI D, ZHU W H, WU Y Z. D-A-π-A organic dyes with fluorenyl-substituted bulky donor for efficient dye-sensitized solar cells[J]. Green Chem Eng, 2023, 4(4): 393-398.

[4] LIU X Y, YU M J, HUANG K, HUANG H Y, GU H X, TIAN C H, QI J, GUO Z Q, LIAN C, WU Y Z, ZHANG W W, ZHU W H. Efficient quasi-homogenous photocatalysis enabled by molecular nanophotocatalysts with donor-acceptor motif[J]. Adv Mater, 2025, 37(4): 2413440.

[5] BANERJEE T, PODJASKI F, KROGER J, BISWAL B P, LOTSCH B. Polymer photocatalysts for solar-to-chemical energy conversion[J]. Nat Rev Mater, 2021, 6: 168-190.

[6] CHENG J Z, CHENG B, XU J S, YU J G, CAO S W. Organic-inorganic S-scheme heterojunction photocatalysts: Design, synthesis, applications, and challenges[J/OL]. eScience, [2024-12-25]. https://doi.org/10.1016/j.esci.2024.100354.

[7] WU J X, YU J J, FAN F, LI R H, WANG M X, LI G, WANG Y T, CUI Y P, LIU D Q, WANG Y J, YAO W Q. Constructing potassium and hydroxyl co-doped dual-dipole structures on highly active 3D g-$C_3N_4$ surfaces for highly boosting photocatalytic hydrogen peroxide production efficiency in pure water[J/OL]. Green Chem Eng, [2024-08-20]. https://doi.org/10.1016/j.gce.2024.08.006.

[8] ZHAO D M, WANG Y Q, DONG C L, HUANG Y C, CHEN J, XUE F, SHEN S H, GUO L J. Boron-doped nitrogen-deficient carbon nitride-based Z-scheme heterostructures for photocatalytic overall water splitting[J]. Nat Energy, 2021, 6: 388-397.

[9] LIN L H, LIN Z Y, ZHANG J, CAI X, LIN W, YU Z Y, WANG X C. Molecular-level insights on the reactive facet of carbon nitride single crystals photocatalysing overall water splitting[J]. Nat Catal, 2020, 3: 649-655.

[10] JI G P, ZHAO Y F, LIU Z M. Design of porous organic polymer catalysts for transformation of carbon dioxide[J]. Green Chem Eng, 2022, 3(2): 96-110.

[11] BAI Y, LI C, LIU L J, YAMAGUCHI Y, BAHRI M, YANG H F, GARDNER A, ZWIJNENBURG M A, BROWNING N D, COWAN A J, KUDO A, COOPER A I, SPRICK R S. Photocatalytic overall water splitting under visible light enabled by a particulate conjugated polymer loaded with palladium and iridium[J]. Angew Chem Int Edit, 2022, 134(26): e202201299.

[12] YE H N, WANG Z Q, HU K, WU W J, GONG X Q, HUA J L. FeOOH photo-deposited perylene linear polymer with accelerated charge separation for photocatalytic overall water splitting [J]. Sci China Chem, 2022, 65: 170-181.
[13] AITCHISON C M, GONZALEZ-CARRERO S, YAO S L, BENKERT M, DING Z Y, YOUNG N P, WILLNER B, MORUZZI F, LIN Y B, TIAN J F, NELLIST P D, DURRANT J R, MCCULLOCH I. Templated 2D polymer heterojunctions for improved photocatalytic hydrogen production [J]. Adv Mater, 2024, 36(20): e2300037.
[14] HAN C Z, XIANG S H, XIE P X, DONG P H, SHU C, ZHANG C, JIANG J X. A universal strategy for boosting hydrogen evolution activity of polymer photocatalysts under visible light by inserting a narrow-band-gap spacer between donor and acceptor [J]. Adv Funct Mater, 2022, 32(16): 2109423.
[15] SHU C, HAN C Z, YANG X Y, ZHANG C, CHEN Y, REN S J, WANG F, HUANG F, JIANG J X. Boosting the photocatalytic hydrogen evolution activity for D-π-A conjugated microporous polymers by statistical copolymerization [J]. Adv Mater, 2021, 33(26): 2008498.
[16] XU T, WANG Z Q, ZHANG W W, AN S H, WEI L, GUO S M, HUANG Y L, JIANG S, ZHU M H, ZHANG Y B, ZHU W H. Constructing photocatalytic covalent organic frameworks with aliphatic linkers [J]. J Am Chem Soc, 2024, 146(29): 20107-20115.
[17] ZAHNG Z, XU Y X. Hydrothermal synthesis of highly crystalline zwitterionic vinylene-linked covalent organic frameworks with exceptional photocatalytic properties [J]. J Am Chem Soc, 2023, 145(46): 25222-25232.
[18] ZHANG W W, CHEN L J, DAI S, ZHAO C X, MA C, WEI L, ZHU M H, CHONG S Y, YANG H F, LIU L J, BAI Y, YU M J, XU Y J, ZHU X W, ZHU Q, AN S H, SPRICK R S, LITTLE M A, WU X F, JIANG S, WU Y Z, ZHANG Y B, TIAN H, ZHU W H, COOPER A I. Reconstructed covalent organic frameworks [J]. Nature, 2022, 604: 72-79.
[19] LI C Z, LIU J L, LI H, WU K F, WANG J H, YANG Q H. Covalent organic frameworks with high quantum efficiency in sacrificial photocatalytic hydrogen evolution [J]. Nat Commun, 2022, 13: 2357.
[20] LAN Z A, WU M, FANG Z P, CHI X, CHEN X, ZHANG Y F, WANG X C. A fully coplanar donor-acceptor polymeric semiconductor with promoted charge separation kinetics for photochemistry [J]. Angew Chem Int Edit, 2021, 60(30): 16355-16359.
[21] YU M J, ZHANG W W, LIU X Y, ZHAO G H, DU J, WU Y Z, ZHU W H. Energy transfer enhanced photocatalytic hydrogen evolution in organic heterostructure nanoparticles via flash nanoprecipitation processing [J]. Green Energy Environ, 2025, 10(2): 390-398.
[22] YU M J, ZHANG W W, GUO Z Q, WU Y Z, ZHU W H. Engineering nanoparticulate organic photocatalysts via a scalable flash nanoprecipitation process for efficient hydrogen production [J]. Angew Chem Int Edit, 2021, 60(28): 15590-15597.
[23] NAJIAFOV H, LEE B, ZHOU Q, FELDMAN L C, PODZOROV V. Observation of long-range exciton diffusion in highly ordered organic semiconductors [J]. Nat Mater, 2010, 9: 938-943.
[24] AITCHISON C M, SPRICK R S. Conjugated nanomaterials for solar fuel production [J]. Nanoscale, 2021, 13(2): 634-646.
[25] MIKHNENKO O V, BLOM P W M, NGUYEN T Q. Exciton diffusion in organic semiconductors [J]. Energ Environ Sci, 2015, 8(7): 1867-1888.
[26] LIU A J, WANG S C, SONG H W, LIU Y W, GEDDA L, EDWARDS K, HAMMARSTROM L, TIAN H N. Excited-state and charge-carrier dynamics in binary conjugated polymer dots towards efficient photocatalytic hydrogen evolution [J]. Phys Chem Chem Phys, 2023, 25(4): 2935-2945.
[27] ZHU Y F, ZHANG Z Z, SI W Q, SUN Q L, CAI G L, LI Y W, JIA Y X, LU X W, XU W G, ZHANG S M, LIN Y Z. Organic photovoltaic catalyst with extended exciton diffusion for high-performance solar hydrogen evolution [J]. J Am Chem Soc, 2022, 144(28): 12747-12755.
[28] BAI Y Q, HU Z C, JIANG J X, HUANG F. Hydrophilic conjugated materials for photocatalytic hydrogen evolution [J]. Chem Asian J, 2020, 15(12): 1780-1790.
[29] HU Z C, WANG Z F, ZHANG X, TANG H R, LIU X C, HUANG F, CAO Y. Conjugated polymers with oligoethylene glycol side chains for improved photocatalytic hydrogen evolution [J]. iScience, 2019, 13: 33-42.
[30] LI A, ZHANG P, KAN E J, GONG J L. Wettability adjustment to enhance mass transfer for heterogeneous electrocatalysis and photocatalysis [J]. eScience, 2024, 4(1): 100157.
[31] HILLMAN S A J, SPRICK R S, PEARCE D, WOODS D J, SIT W Y, SHI X Y, COOPER A I, DURRANT J R, NELSON J. Why do sulfone-containing polymer photocatalysts work so well for sacrificial hydrogen evolution from water [J]. J Am Chem Soc, 2022, 144(42): 19382-19395.
[32] HU X L, YANG X J, SONG B Y, ZHAN Z, SUN R X, GUO Y T, YANG L M, YANG X, ZHANG C, HUSSAIN I, WANG X Y, TAN B E. Sulfone-functionalized stable molecular single crystals for photocatalytic hydrogen evolution [J]. Susmat, 2024, 4(3): e220.
[33] KOSCO J, GONZALEZ-CARRERO S, HOWELLS C T, ZHANG W M, MOSER M, SHEELAMANTHULA R, ZHAO L G, WILLNER B, HIDALGO T C, FABER H, PURUSHOTHAMAN B, SACHS M, CHA H J, SOUGRAT R, ANTHOPOULOS T D, INAL S, DURRANT J R, MCCULLOCH I. Oligoethylene glycol side chains increase charge generation in organic semiconductor

nanoparticles for enhanced photocatalytic hydrogen evolution [J]. Adv Mater, 2021, 34(22): 2105007.

[34] WOODS D J, HILLMAN S A J, PEARCE D, WILBRAHAM L, FLAGG L Q, DUFFY W, MCCULLOCH I, DURRANT J R, GUILBERT A A Y, ZWIJNENBURG M A, SPRICK R S, NELSON J, COOPER A I. Side-chain tuning in conjugated polymer photocatalysts for improved hydrogen production from water [J]. Energ Environ Sci, 2020, 13(6): 1843-1855.

[35] XU J Y, LI W L, LIU W X, JING J F, ZHANG K F, LIU L P, YANG J, ZHU E W, LI J S, ZHU Y F. Efficient photocatalytic hydrogen and oxygen evolution by side-group engineered benzodiimidazole oligomers with strong built-in electric fields and short-range crystallinity [J]. Angew Chem Int Edit, 2022, 61(45): e202212243.

[36] HU Z C, ZHANG X, YIN Q W, LIU X C, JIANG X F, CHEN Z M, YANG X F, HUANG F, CAO Y. Highly efficient photocatalytic hydrogen evolution from water-soluble conjugated polyelectrolytes [J]. Nano Energy, 2019, 60: 775-783.

[37] CHANG C L, LIN W C, TING L Y, SHIH C H, CHEN S Y, HUANG T F, TATENO H, JAYAKUMAR J, JAO W Y, TAI C W, CHU C Y, CHEN C W, YU C H, LU Y J, HU C C, ELEWA A M, MOCHIZUKI T, CHOU H H. Main-chain engineering of polymer photocatalysts with hydrophilic non-conjugated segments for visible-light-driven hydrogen evolution [J]. Nat Commun, 2022, 13: 5460.

[38] DING H R, CHU Y M, XU M Y, ZHANG S C, YE H R, HU Y, HUA J L. Effect of π-bridge groups based on indeno-[1, 2-b]thiophene D-A-π-A sensitizers on the performance of dye-sensitized solar cells and photocatalytic hydrogen evolution [J]. J Mater Chem C, 2020, 8(42): 14864-14872.

[39] AITCHISON C M, SPRICK R S, COOPER A I. Emulsion polymerization derived organic photocatalysts for improved light-driven hydrogen evolution [J]. J Mater Chem A, 2019, 7(6): 2490-2496.

[40] LIU Y X, WU J, WANG F. Dibenzothiophene-S, S-dioxide-containing conjugated polymer with hydrogen evolution rate up to 147 mmol $g^{-1}$ $h^{-1}$ [J]. Appl Catal B: Environ, 2022, 307(15): 121144.

[41] LIN W C, JAYAKUMAR J, CHANG C L, TING L Y, ELSAYED M H, ABDELLAH M, ZHENG K B, ELEWA A M, LIN Y T, LIU J J, WANG W S, LU C Y, CHOU H H. Effect of energy bandgap and sacrificial agents of cyclopentadithiophene-based polymers for enhanced photocatalytic hydrogen evolution [J]. Appl Catal B: Environ, 2021, 298(5): 120577.

[42] YANG T Y, ZHU E W, GUO H Y, DU J, WU Y Y, LIU C B, CHE G B. Visible light-driven D-A conjugated linear polymer and its coating for dual highly efficient photocatalytic degradation and disinfection [J]. ACS Appl Mater Interfaces, 2021, 13(43): 51447-51458.

[43] YANG H F, LI C, LIU T, FELLOWES T, CHONG S Y, CATALANO L, BAHRI M, ZHANG W W, XU Y J, LIU L J, ZHAO W, GARDNER A M, CLOWES R, BROWNING N D, LI X B, COWAN A J, COOPER A I. Packing-induced selectivity switching in molecular nanoparticle photocatalysts for hydrogen and hydrogen peroxide production [J]. Nat Nanotechnol, 2023, 18: 307-315.

[44] ZHU X L, JIA Y H, LIU Y H, XU J Y, HE H R, WANG S Y, SHAO Y, ZHAI Y X, ZHU Y F. Enhancing built-in electric fields via molecular symmetry modulation in supramolecular photocatalysts for highly efficient photocatalytic hydrogen evolution [J]. Angew Chem Int Edit, 2024, 63(26): e202405962.

[45] WANG Z Q, DING G X, HUANG H W, ZHANG J T, LV Q, SHUAI L, NI Y H, LIAO G F. Unraveling the dipole field in ultrathin, porous, and defective carbon nitride nanosheets for record-high piezo-photocatalytic $H_2O_2$ production[J/OL]. eScience, [2024-12-24]. https://doi.org/10.10106/j.esci. 2024. 100370.

[46] LU T, CHEN F W. Multiwfn: A multifunctional wavefunction analyzer [J]. J Comput Chem, 2011, 33(5): 580-592.

[47] ZHANG J, LU T. Efficient evaluation of electrostatic potential with computerized optimized code [J]. Phys Chem Chem Phys, 2021, 23(36): 20323-20328.

[48] SACHS M, SPRICK R S, PEARCE D, HILLMAN S A J, MONTI A, GUILBERT A A Y, BROWNBILL N J, DIMITROV S, SHI X Y, BLANC F, ZWIJNENBURG M A, NELSON J, DURRANT J R, COOPER A I. Understanding structure-activity relationships in linear polymer photocatalysts for hydrogen evolution [J]. Nat Commun, 2018, 9: 4968.

[49] HU W, LIN L, ZHANG R Q, YANG C, YANG J L. Highly efficient photocatalytic water splitting over edge-modified phosphorene nanoribbons [J]. J Am Chem Soc, 2017, 139(43): 15429-15436.

（责任编辑：刘亚萍）